European Scholar Journal (ESJ)
Available Online at: https://www.scholarzest.com
Vol. 3 No.9, September 2022
ISSN: 2660-5562

INFLUENCE OF EXB DRIFT WAVE INSTABLITY IN HOLLOW MAGNETRON SPUTTERING PARAMETERS

Alaa.K. Bard [1] , Qusay. A. Abbas[1]
[1]Physics Dep., College of Science, University of Baghdad, Baghdad, Iraq
*__Email__: alaakhamees91@gmail.com

Article history:

Received: 30th June 2022
Accepted: 28th July 2022
Published: 4th September 2022

Abstract:

In the present paper, the effect of the EXB drift wave instability on the hollow magnetron sputtering parameter in the present of axial magnetic field was described in details. The plasma parameters of the normal glow discharge region are diagnostic. The discharge properties were examined using spectroscopic measurements of the plasma created inside the chamber and the Boltzmann diagram to determine the electron temperature. The results showed that adjusting the coil current changes the discharge properties. The properties of the plasma increase with the rise in the coil current, electron temperature (Te), Debye length (D) and electron number density (ne).

Keywords: *Cylindrical magnetron, hollow magnetron, plasma parameters*

1.INTRODUCTION

Bartels and Paschen developed the hollow cathode (HC) discharge by accident more than a century ago [1]. Hollow cathode discharges are commonly used in atomic spectroscopy , as UV generators, and in laser technology [2-4]. Since Thornton and Penfold's invention [5], inverted cylindrical magnets (ICM) with DC, pulsed or alternating current have been used. They are used to deposit thin films either on fibers and wires [6-8] or on objects of complex shapes [9, 10]. which gives satisfactory results in terms of deposition rate and thickness uniformity. A hollow cathode is a cylindrical tube that is open on both ends or closed on one end. Other designs, such as two flat electrodes placed close together, are also possible [11, 12]. Magnetron mist (MS) discharges are of interest from a fundamental and applied point of view [13,14]. MS discharges use a magnetic field to enhance the plasma density in front of the negatively biased cathode. The main application is the deposition of functional films composed of cathode spray material. Magnetron sputtering is one interesting method for thin-film deposition. In 1974 Chappins invented a magnetron to improve the spraying process [15]. Without the magnetron, the system was limited to low ionization, low sedimentation, unstable plasma etc., [16, 17]. These limitations are overcome by the magnetron as electrons can be trapped towards the cathode region and ionization increase [18]. Various configurations of magnetrons have been used such as flat, cylindrical, and shotgun designs [19]. A common aspect of all these configurations is the electron trapped in the presence of the electric cross magnetic field drift. The magnetron is an important unit responsible for the particle behavior in magnetron DCs. It is important to understand the particle behavior due to magnetrons in plasma [20,21]. In recent years, the study of magnetic field distribution and its effect on plasma parameters has gained importance to improve the quality of thin films [22] - field distribution in axial and radial positions causes changes in plasma parameters such as electron temperature and density [23,24]. EXB devices have recently been popular in a variety of aerospace and industrial applications, including electric propulsion, semiconductor processing, and plasma mass filtration[25-27]. External electric and magnetic fields can regulate the route of electrons and ions in EXB setups. The generation of a self-generated electric voltage in the plasma column is a fundamental feature of EXB devices[28-33]. A drift motion with magnetic drift is one of the causes of a self-generated electric potential, which involves complex physics such as long-wave instability and anomalous transport[34-38]. As a result, characterization of the devices requires a thorough understanding of the dipole electric field of the plasma column caused by externally applied elements. In this work, the influence of EXB drift wave instability in hollow magnetron sputtering parameters.

EXPERIMENTAL SET UP

A vacuum-compatible stainless steel chamber, aluminum target electrode, coil, pumping system, DC power supply, and other components make up the experimental setup. The stainless steel chamber is hollow cylindrical in shape, measuring 25 cm in diameter and 22 cm in length. This cylindrical chamber serves as one of two electrodes (the other being an external electrode) required for plasma generation. Along the vacuum chamber's vertical axis, a 3 cm diameter and 18 cm length aluminum rod was inserted in the middle. As an internal electrode, this rod-shaped

electrode is used. Figure 1 shows a schematic illustration of this cylindrical axial electrode layout. To prevent the loss of energetic electrons, limiters are linked to both ends of the inner electrode. The inner electrode (aluminum rod) serves as the positive electrode, while the outside electrode (chamber) serves as the negative electrode in an hollow magnetron discharge. Figure 1 also includes a schematic diagram of this setup.

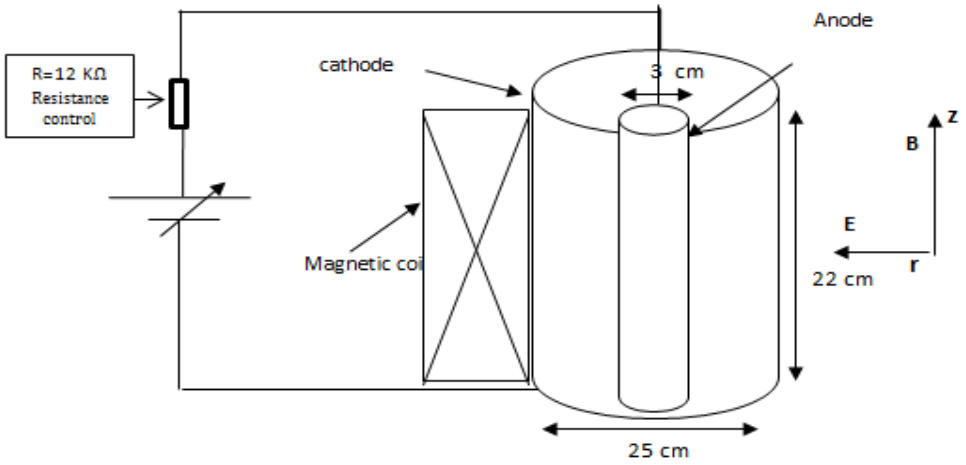

Figure 1.show The diagram of Inverted configuration in cylindrical magnetron sputtering

The coil is designed to produce a consistent magnetic field inside the discharge vessel in a direction parallel to the central pole's longest axis, as illustrated in the figure (2).This figure shows that the magnetic field has maximum values in the central region. The size of this field increases as the file flow increases. Argon gas was used to create the plasma. For the plasma formation, The operational pressure (0.4 Torr) was increased from the fundamental pressure inside the vacuum vessel, and argon gas was delivered through a gas dosing valve. To generate the plasma, a DC power source (3000 V, 1 A) was employed to bias the electrodes.

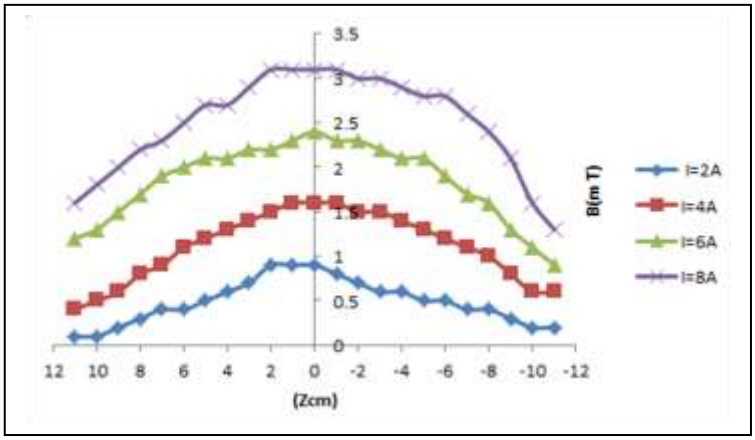

Figure 2. The calculated magnetic field behavior as a function of coil currents.

3. THEORETICAL DESCRIPTION OF PLASMA PARAMETERS

The electric field in the radial direction can be calculated according to the cylindrical coordinate as [39,40]:

$$E_r = \frac{1}{r}\frac{V_{ab}}{Ln\left(\frac{b}{a}\right)} \qquad (1)$$

where Vab, a, and b are the potential between two the electrodes, radius of the inner cylinder, and radius of the outer cylinder, respectively.

The presence of magnetic field in magnetron device will generate Lorentz force. This force causes a circular motion of the electrons and ions with cyclotron frequency that is calculate by using the equation [41]:

$$\omega_c = {|qB|}/{m} \qquad (2)$$

In the magnetron configuration, the magnetic field (in the Z direction (B_z)) is perpendicular to the electric field (in the r direction(E_r)), and the drift velocity of EXB is in the azimuthal direction. We can calculate from equation:

$$v_{(EXB)\theta} = \frac{E_r}{B_z} \qquad (3)$$

the electron temperature (T_e) is The most crucial component used for describing a plasmas state. T_e can be calculated according to the method of the Boltzmann diagram as follows [42,43]:

$$\ln\left(\frac{I_z\lambda_{Ki,z}}{g_{K,Z}A_{Ki,Z}}\right) = -\frac{1}{k_BT_e}E_{k,z} + \ln\left(\frac{hcL_{nZ}}{4\pi P_Z}\right) \quad (4)$$

Where where Z, h, c, k_B, E_{kZ}, g_{kZ}, P_Z, and I_Z are represent the species-related ionization state, plank constant, speed of light, constant of Boltzmann, the top energy level's energy k, higher energy level degeneration k, in the ionization step Z reflects the species partition function, and the integrated optical intensity of a species in the ionization stage Z, respectively. Anyway, if the left-hand side amount of Equation (3) is plotted for several transformations against the higher-level energy of the species in the Z ionization phase, then the equation produces a line diagram. As a result, the slope of the line graph represents Te in eV. Also, using a stark expansion relationship to calculate the electron number density assuming that the stark expansion is the dominant effect [44] :

$$n_e cm^{-3} = \left[\frac{\Delta\lambda}{2\omega_s(\lambda_D T_e)}\right]N_r \quad (5)$$

where ω_s represent the Stark expansion parameter , Δλ represents the full width at half maximum of the line , while N_r represents the reference electron number density, which is equal to 10^{16} cm^{-3} for neutral atoms and 10^{17} cm^{-3} for singly charged ions.

When a plasma is subjected to a local potential, the oppositely charged particles organize to confine the electric field (**E**). The potential resulting from the thermal oscillation of highly mobile electrons is shielded to a distance called the Debye length (λ_D). The Debye length in the plasma can be obtained by equality the kinetic energy of the thermal electrons with resulting electrostatic potential as follows [45]:

$$\lambda_D = \sqrt{\frac{\varepsilon_0 k_B T_e}{e^2 n_e}} \quad (6)$$

Where k_B is Boltzmann's constant , ε_0 is the permittivity of free space, e is the electronic charge , T_e is the electron temperature and n_e the electron number density.

4. RESULTS AND DISCUSSION

4.1 Glow discharge structure

The device works on the basis of a luminous discharge between the electrodes. When a steady current is provided in this device, the plasma produces an argon discharge corona. Between the two electrodes, a voltage of around 2.4 kV is applied. As a result of this applied voltage, an electric field is generated and causes an electrical failure in the argon gas. When the displayed magnetic field (which is generated from a magnetic coil) is applied tangentially to the electric field while maintaining a glow discharge between the electrodes and the gas pressure used to generate the plasma in this device is (0.4 Tor) and the range of magnetic field values (coil current) The user is 2, 4, 6 and 8 amps. The presence of the electric and magnetic fields together in the magnetron traps electrons near the surface of the cathode (in the region of the strong electric current field). Electrons follow helical paths around magnetic field lines, so they undergo further ionizing collisions with the gaseous neutral near the target's surface. The ions from these collisions lead to a high sedimentation rate. This also means that the plasma can be maintained at low pressure. Figure 3 shows images of the effect of the magnetic current coil on the normal flare regions at a constant pressure of 0.4 Tor in a cylindrical hollow-cathode magnetron device. The discharge regions occurring within the cylindrical cavity, according to this configuration, can carry currents of the order of several amperes at a cathode drop of several hundred volts and in a reasonably cold carrier gas. A significant decrease in the anode was also observed in this configuration. In addition, the cathode has a larger surface area than the anode. Within the hollow cathode, the regions are arranged in a circular pattern. The term "hollow cathode" refers to a low pressure that can be maintained in a vacuum in the presence of a strong magnetic field; Gas is pumped through a hot incandescent cathode cylinder. Simply put, the gas is ionized and heated very effectively in the cathode region, and the resulting plasma flows from there along the magnetic field to the anode, where a significant part of it is recombined. The presence of electrostatic and magnetic fields has been used to produce a very intense and uniform plasma near the target surface.

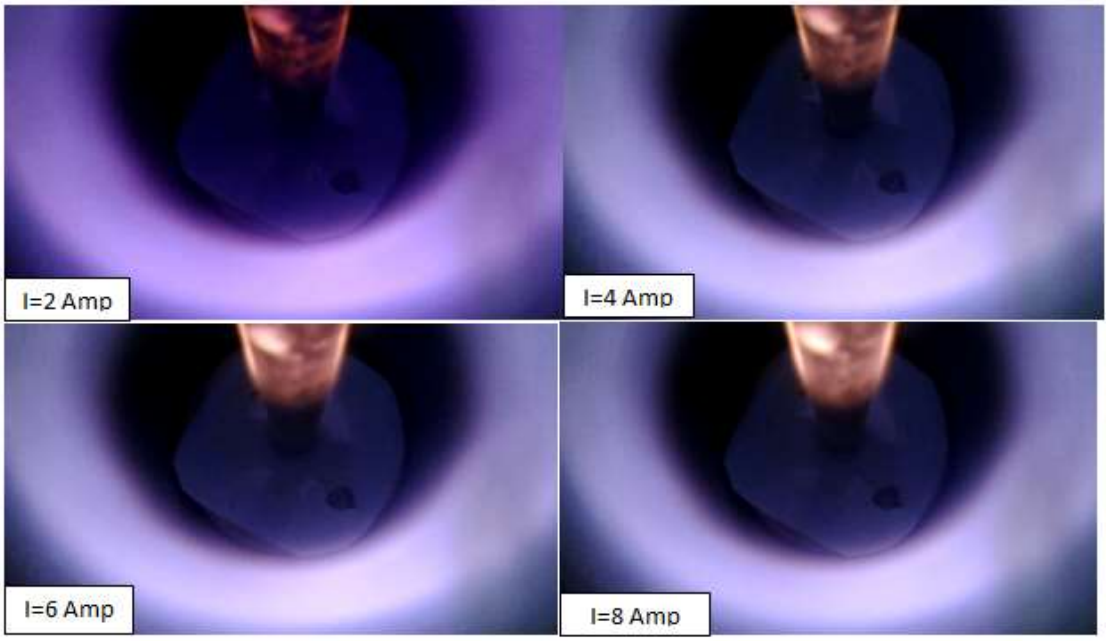

Figure 3. Photographs of glow discharge for different coil currents at constant pressure of 0.4 Torr in inverted cylindrical magnetron device.

4.2 Investigation of the properties of plasma in the natural glow discharge region:

4.2.1 Basic parameters of the magnetron

the effect of magnetic field strength on the plasma parameters of the hollow magnetron sputtering in the normal glow discharge region will be discussed in this section. When the current is constant it produces a normal glow discharge. Between two coaxial cylindrical electrodes, a continuous voltage of around 2.4 kV is delivered. A plasma discharge is created as a result of the external voltage, a space charge is created and then the potential of the electrodes decreases. The magnetic field (which is generated by passing a constant current in the solenoid) is positioned tangential to the direction of the electric field. Figure 4 shows the discharge voltage as a function of the coil current for different pressures. It is quite clear from this figure that the discharge voltage decreases with increasing gas pressure for all values of coil current. This result is due to the increase in the discharge current as the gas pressure of the stator coil current increases. Therefore, the discharge voltage decreases as the gas pressure increases for all coil currents. In addition, it is noted that at constant pressure, the discharge voltage decreases with increasing coil current up to about 6 A, and then the discharge voltage increases. This behavior can be explained as follows: When the coil current is less than 6A, the presence of the magnetic field perpendicular to the electric field increases the path length of the electrons ensuring a sufficiently high ionization rate. Thus, ions are formed and most of these ions are accelerated towards the cathode, causing the atoms of the cathode material to spray out and the secondary electrons to be emitted. These secondary electrons enter the trapping region and cause sufficient ionization to sustain the discharge. Therefore, the discharge current increases and therefore the discharge voltage decreases. This happens for coil currents less than 6A. When the coil current is more than 6A, the magnetic field strength becomes so strong compared to the applied voltage, that the electrons cannot reach the positive pole. Therefore, the probability of electrons colliding with neutral atoms to cause ion bombardment of the cathode will decrease. The discharge current decreases and the discharge voltage increases

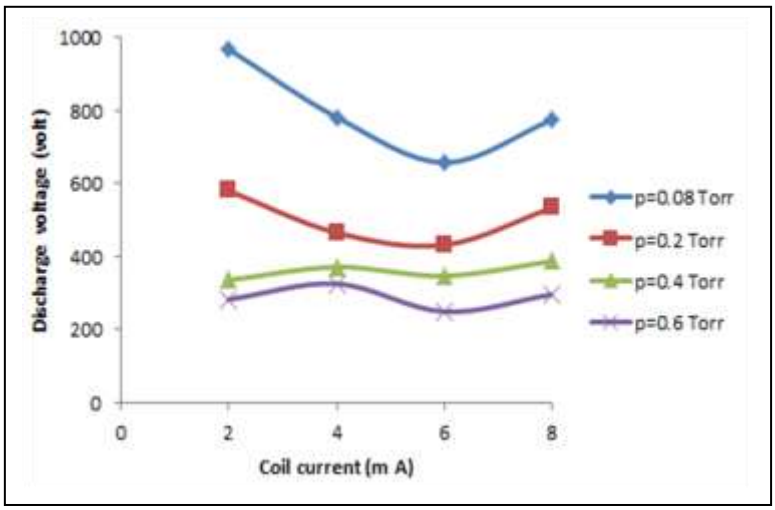

Figure 4. The variation of discharge voltage as a function of coil current for different pressures.

The electric field is calculated using equation (1). It can be shown that the electric field in cylindrical coordinates varies with different radial positions (the irregular field). By taking the empirical data for the discharge voltage at a pressure of 0.4 Torr. From figure (4) and the value of the constants a and b as 12.5 cm and 1.5 cm respectively. Figure 5 shows the variation of the electric field (E_r) as a function of the coil current at different radial positions. From this figure, Many features can be noted from both figures that the electric field has a value reduced with increased of radial positions from inner cylinder

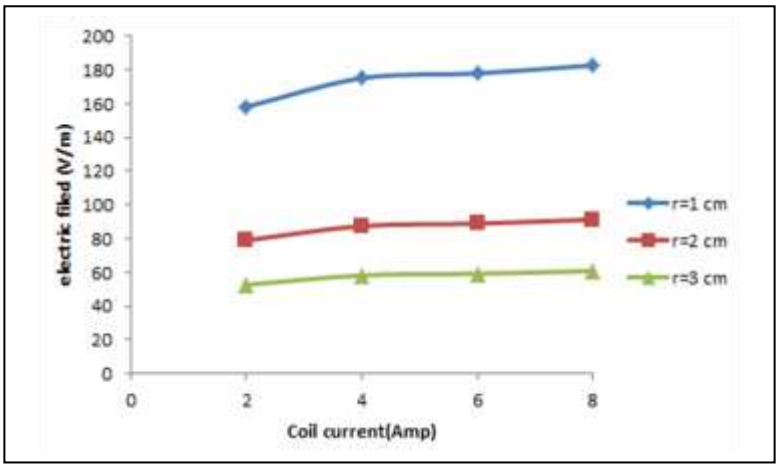

Figure 5. Radial electric filed as a function of coil current for different radial positions from cathode surface at pressure 0.4 Torr.

The cyclotron frequency is calculated using equation (2) and taking the values of electron and argon ion masses as 9.1 × 10-31 kg and 6.62 × 10-26 kg respectively and the experimental data for the magnetic field from Fig. (2). The axial behavior of electron and ion frequencies along the Z direction was plotted as a function of different coil currents as shown in Figures (6) and (7)

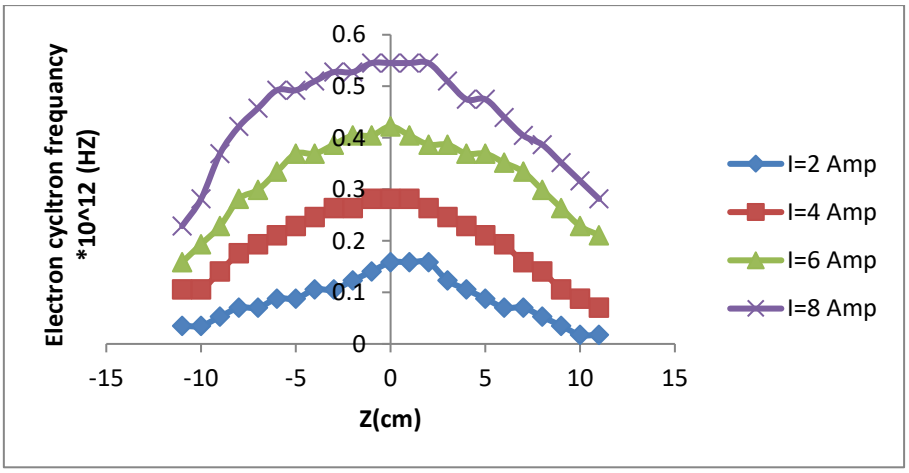

Figure 6. The axial behavior of electrons cyclotron frequency.

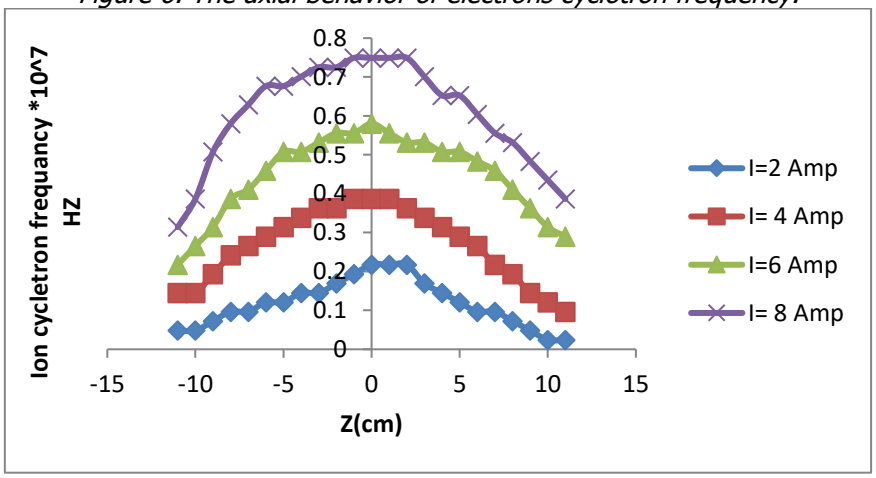

Figure 7. The axial behavior of ions cyclotron frequency.

Figures (6) and (7) show that the cyclotron frequencies of the electrons have greater values than the cyclotron ion frequencies because the mass of the electron is less than the mass of the ion , and decreases towards the ends of the cathode in the magnetron configuration.

Using Equation (3) according to the values of the electric field (Fig. (5)) and magnetic field strength (Fig. (2)), the axial profile of the drift velocity E × B at different radial positions of the inner cylinder is plotted as a hollow cylindrical magnetron configuration in Fig. (8), and it is indicated from the figure that v_{ExB} is very high in the central region near the inner cylinder and lowers towards the ends of the inner cylinder. One can also note that the drift velocity E×B is maximum near the surface inner cylinder which corresponds to the plasma envelope region and is compressed away from the inner cylinder in the radial direction due to the transition that occurs from the envelope to the pre-field region. The significant increase in the drift velocity in the shell region is due to the energy gain of electrons from the electric field of the strong shell at different rates.

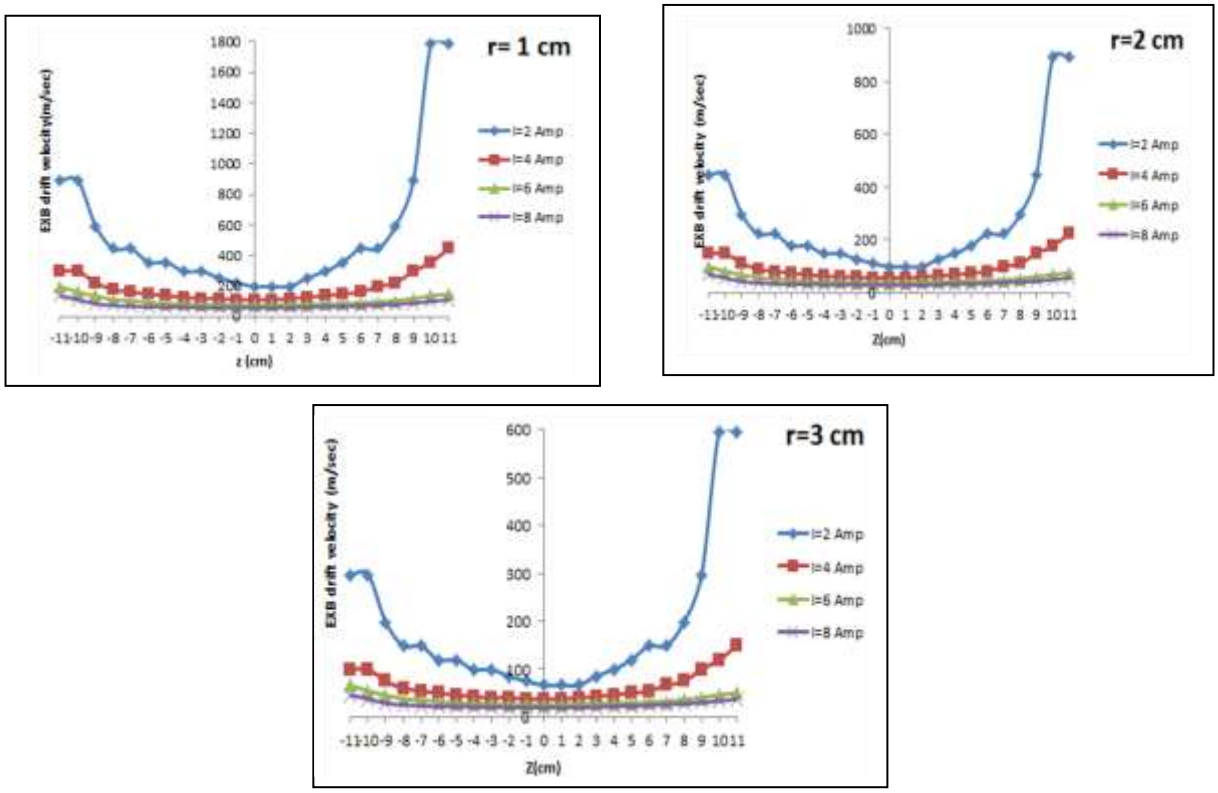

Figure 8. The axial behavior of EXB drift velocity in azimuthal direction versus coil current for different radial positions.

4.3 I-V characteristics

The I (current) - V (voltage) characteristics of the discharge were measured, in an inverted magnetron configuration. It operates in an Ar environment at a pressure of 0.4 Tor, , as well as in four distinct axial magnetic fields ranging from 2 to 8 amperes. The relationship between the discharge current and the discharge voltage is discovered in hollow magnetron discharge under a constant magnetic field and operating pressure. Figure (9) shows the characteristic I-V curve of the inverted configuration. The discharge voltage increases with increasing magnetic field strength (coil current), but the discharge voltage is nearly constant with increasing discharge current, demonstrating a higher level of electron trapping in the discharge. Because the electrons in an inverse magnetron discharge are coupled with an externally applied magnetic field, radial scattering reduces the rate of electron loss. Moreover, Due to the increased surface area of the cathode, secondary electron emission is also quite high in the hollow magnetron discharge.

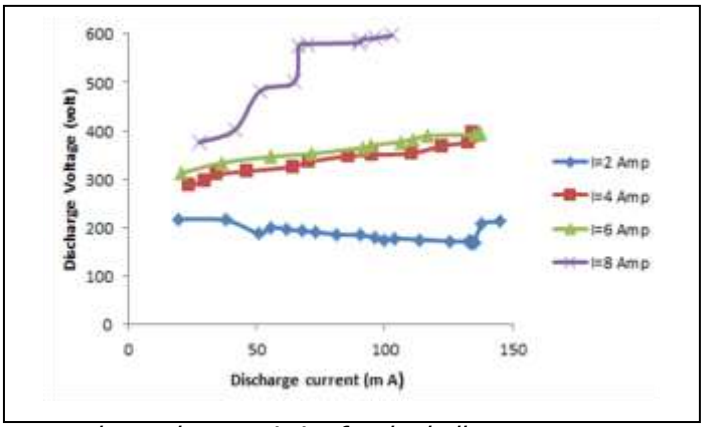

Figure 9. Current–voltage characteristics for the hollow magnetron sputtering .

4.4 Emission spectra of plasma in magnetized hollow cathode

Figure (10) shows the emission spectra of the inverted configuration electrodes in the wavelength region 320-740 nm at a constant argon gas pressure. The spectra show seven emission peaks of neutral argon (ArI) at wavelengths 546.71600, 557.25410, 617.94190, 659.61130, 677.99260, 703.02510, 735.08140 nm and four ionic emission lines of argon (Ar II) at wavelengths (361.18130 ,405.76750 ,427.75280 ,470.23160 nm). according to the spectra, with Increasing the coil current the strength of all peaks in the ArI and ArII lines increases In ArI, the light emission intensity is much lower than the light emission intensity in ArII The intensity of all peaks increases with the increase in the coil current from 2 to 4 A The probability of collision between electrons and atoms the gas increases due to the increase in the density of the number of electrons, which increases with the increase in the current of the coil, allowing the electrons to obtain sufficient excitation energy.

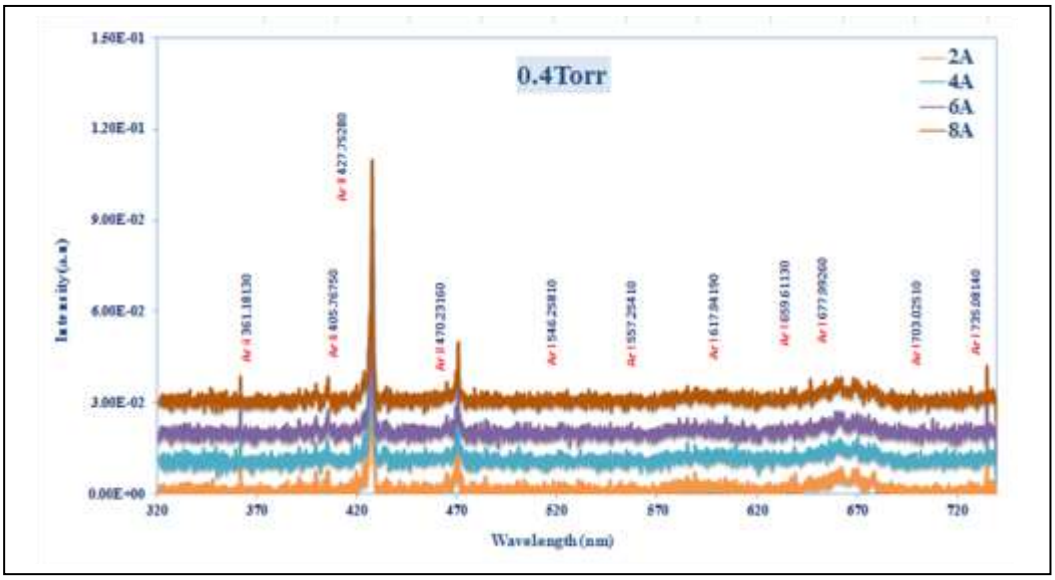

Figure 10. Optical emission spectra of Ar plasma for inverted magnetron sputtering at various coil current.

4.4 Plasma parameters of hollow magnetron sputtering

Electron temperature is the most important parameter of the plasma that is used to describe the state of the plasma .A variety of plasma excitation and ionization processes are controlled by the electron temperature (Te). Assume the plasma is at local thermodynamic equilibrium and the number of excited atoms follows the Boltzmann distribution to compute Te. Using the data in the table(1), the method of Boltzmann plot was used to calculate the value of Te (equation (4)).

Table 1.*Ar I standard lines are used to calculate electron temperature, and their characteristics. [45]*

$\lambda(\mathbf{nm})$	$\mathbf{A_{ji}g_i}$	$\mathbf{E_i(eV)}$	$\mathbf{E_j(eV)}$	**ion**
546.71600	38×10^6	13.09487256	15.3620414	ArI
557.25410	4.6×10^6	13.09487256	15.31916801	ArI
617.94190	0.2×10^6	13.30222747	15.30807770	ArI
659.61130	0.11×10^6	13.07571571	14.95485204	ArI
677.99260	0.363×10^6	13.47988682	15.30807770	ArI
703.02510	13.4×10^6	13.07571571	14.83881100	ArI
735.08140	1.2×10^6	13.32785705	15.0140655	ArI

Figures (11) show the Boltzmann diagram approach to hollow magnetron atomization using specific argon atomic lines (ArI) at the positions under investigation at different gas pressures.

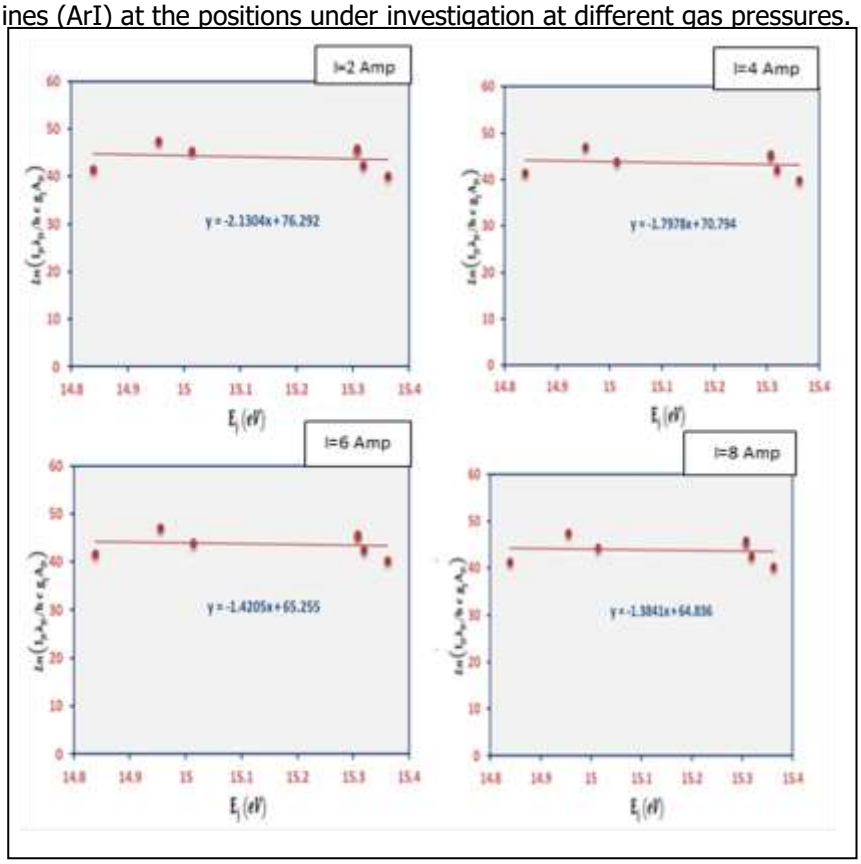

Figure 11. the Boltzmann diagram approach to hollow magnetron electrodes using selected atomic argon (ArI) lines at a different coil current.

One of the most reliable techniques for determining electron number density (ne) is the use of atomic spectroscopy lines emitted from the plasma. Equation (5) can be used to calculate the electron number density, which is called the Stark expansion effect. The FWHM (full width at half maximum) values were used to calculate the electron number density using the Stark effect depending on the measured standard values for this line (Nr = $10^{16}cm^{-3}$) [46]. The effect of coil current on the behavior of electron number density and electron temperature is shown in Figure (12) in the hollow magnetron sputtering device . The curve showed an increase in the value of both the electron number density and the electron temperature with increase of the coil current from 2 Amp to 8 Amp. This behavior can be explained as; with increasing of coil current the plasma confinement was increased which cause to make more inelastic collisions between plasma particles with neutral atoms in the region near from inner electrode surface and this make increasing of electron number density .

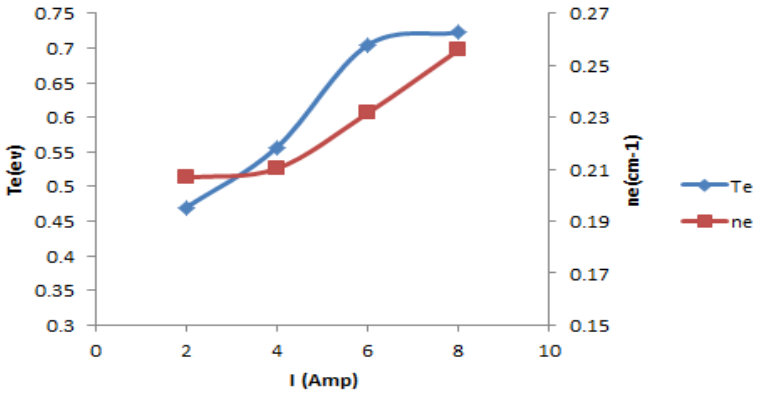

Figure 12. The contrast of ne and Te in hollow magnetron sputtering as a function of coil current

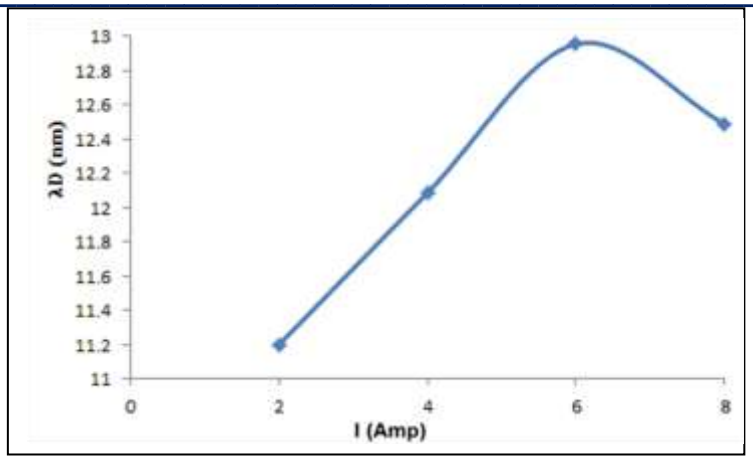

Figure 13. the variation of λD against the coil current in hollow magnetron sputtering.

The Debye length (λD) was also calculated using equation (6) and exhibit in figure (13), from figure showed that the Debye length increases with increasing coil current in the hollow magnetron sputtering. The density of electrons is large, so the Debye length is also large.

5.CONCLUSIONS

The plasma parameters of the formation of the hollow cylindrical magnetron are described in more detail. The magnetic field generated by magnetron production can control the trajectory of ions and electrons in the plasma. The magnetic field distribution has a great influence on the properties of the plasma and the sedimentation rate at various axial and radial positions. The contrast of the discharge regions of the normal glow with the coil currents in a hollow cylindrical magnetron was studied and the discharge properties were examined using spectroscopic measurements of the plasma generated inside the chamber. According to the axial profile of the magnetic field, the axial profile of the drift velocity E × B and cyclotron frequency has a minimum value in the central region of the anode electrode and becomes maximum at the ends of the anode electrode in a hollow configuration. Electron temperature and electron number density are found to increase with increasing coil current but wavelength decreases with increasing coil current in hollow cylindrical magnetron.

REFERENCES

1. [1] Paschen F and Heliumlinien B 1916 Ann. Phys. 355 901
2. [2] Hagelaar G J M, Mihailova D B and van Dijk J 2010 J. Phys. D:Appl. Phys. 43 465204
3. [3] Duquette D W and Lawler J E 1982 Phys. Rev. A 26 330
4. [4] Ishikawa D and Hasegawa S 2019 J. Spectrosc. 2019 1–6
5. [5] Thornton J A and Penfold A S 1979 Cylindrical magnetron sputtering Thin Film Processes ed J L Vossen and W Kern (London: Academic) pp 75–113
6. [6] Petrov I G, Kourtev J S and Orlinov V I 1986 An estimation for the possibilities of the cylindrical magnetron systems for coating of wires Bulg. J. Phys. 13 273–9
7. [7] Kaneko T and Nittono O 1997 Improved design of inverted magnetrons used for deposition of thin films on wires Surf. Coat. Technol. 90 268–74
8. [8] Amberg M, Geerk J, Keller K and Fischer A 2004 Design, characterisation and operation of an inverted cylindrical magnetron for metal deposition Plasma Devices Oper.12,86-175.
9. [9] Glocker D A 1995 Principles and applications of hollow cathode magnetron sputtering sources Soc. Vacuum Coaters 38 298–302.
10. [10] Siegrfired D E, Cook D and Glocker D 1996 Reactive cylindrical magnetron deposition of Titanium nitride and zirconium nitride films Soc. Vacuum Coaters 39 97–101.
11. [11] Koch H, Friedrich L J, Hinkel V, Ludwig F, Politt B and Schurig T 1991 J. Vac. Sci. Technol. A 9 2374.
12. [12] Jacobsen H 2007 Integration von piezoelektrischen Dünnschichten in einen MEMS kompatiblen Prozessablauf aufWaferebene PhD Thesis (Christian-Albrechts-Universit¨atzu Kiel, Germany)
13. [13] Ellmer K 2008 Low Temperature Plasmas ed et al (New York: Wiley) p 675
14. [14] Gudmundsson J T 2020 Plasma Sources Sci. Technol. 29 113001.
15. [15] John S. Chapin, Boulder, Colo, "Sputtering Process and Apparatus ,"United States Patent, 4,166,018",Aug. 1979.
16. [16] P.J. Kelly, R.D. Arnell, "Magnetron sputtering: a review of recent developmentsand applications,"Vacuum., vol. 56, no. 3, pp.159-172, Mar.2000.
17. [17] J. Musil"Recent advances in magnetron sputtering technology", "Surface and Coatings Technology," vol.100 – 101, PP.280-286, Mar 1998.

18. [18] Matthew J. Goeckner, Johm A. Goree, and Torrence E. Sherdian, Jr ,."Monte Carlo Simulation of Ions in a Magnetron Plasma,"IEEE Trans. Plasma Sci, vol. 19, no. 2, pp. 301-308, Apr. 1991.
19. [19] T. E. Sherdian and J. Goree, " Low-frequency turbulent transport in magnetron plasmas", J. Vac. Sci. Technol. A, vol. 7, no. 3, pp.1014-1018, Oct. 1989.
20. [20] Wu, S. Z., "Dependence of plasma characteristics on dc magnetron sputter parameters", Journal of Applied Physics, vol. 98, no.8, p. 083301,Oct 2005.
21. [21] M. Dimitrova, T. K. Popov, J. Todorovand, and T. G. Naydenova ,"Second derivative Langmuir probe measurements in Faraday dark space in Argon d.c. gas discharge at intermediate pressures," J. Phys. Conf. Ser., vol ,44 .pp. 169–174, Jul. 2006.
22. [22] K. Honglertkongsakul, S. Chaiyakun, N. Witit-anun, W. Kongsri, and P. Limsuwan, "Single Langmuir Probe Measurements in an Unbalanced Magnetron Sputtering System," Procedia Eng., vol. 32, pp. 962–968, Jan. 2012.
23. [23] S. M. Borah, A. R. Pal, H. Bailung, and J. Chutia, "Effect of E × B electron drift and plasma discharge in dc magnetron sputtering plasma", Chinese Phys. B, vol. 20, no. 1, p. 014701, Jan. 2011.
24. [24] B. Crowley, D. Homfray, U. Fantz, D. Boilson, and R. S. Hemsworth" ,Electron Energy Distribution Function Measurements by Langmuir Probe in ITER like Negative Ion Sources," AIP Conf. Proc., vol. 925, no. 1, pp. 193– 207, Sep. 2007.
25. [25] Kaganovich, A. Smolyakov, Y. Ritsis, E. Ahido, I. J. Michaelides, P. Gornes, F. Taccogna, R. Gueroult, S. Tsikata, A. Bourdon, J.-P. Buff, M. Kedar, A.; T. Boyce, M. Merino, M. Capelli, K. Hara, J. A. Carlson, N. J. Fish, P. Chabert, Schweigert, T. Lafleur, K. Matias, AV. Khrabrov, R.W. Boswell, and A.; Fruchtman, "The physics of E×B discharges related to plasma propulsion and the like Technologies," Phys. Plasma 27 (12), 120601 (2020).
26. [26] i. Levchenko, S. Xu, S. Mazouffre, D. Lev, D. Pedrini, D. Goebel, L. Garrigues, F. Taccogna and K. Bazaka, "New Perspectives, Frontiers, and Perspectives for Plasma Space Electric Propulsion," Phys.Plasma 27(2), 020601 (2020).
27. [27] kilos. Takahashi, "Radio-frequency thrust-type helicon and magnetic plasmas Plasma nozzles" Rev. Mod. Plasma Phys. 3, 3 (2019).
28. [28] The Physics and Technology of Ion Sources, edited by I.G. Brown (Wiley, New York, 2004).
29. [29] J.-P. Boeuf, "Rotating structures in magnetized low-temperature plasmas— Insight from particle simulation, "Front. Plasma Phys. 2, 74 (2014).
30. [30] J. Y. Kim, K. S. Chung, S. Kim, J. H. Ryu, K.-J. Chung and ES Hwang, Thermodynamics of a magnetically expanding plasma with isothermal behavior Trapped Electrons" New J. Phys. 20, 063033 (2018).
31. [31] J. Y. Kim, J. Y. Jang, K. S. Chung, K.-J. Chung and YS Hwang, "Timedependent Kinetic analysis of electrons trapped in magnetic expansion Plasma," Plasma Sources Science. Technol. 28, 07LT01 (2019).
32. [32] s. Correyero, J. Jarrige, D. Packan, and E. Ahedo, "Plasma beam characterization Along the magnetic nozzle of an ECR motor," Plasma Sources Sci. Technol. 28, `095004 (2019).
33. [33] k. Takahashi, "Magnetic crater approaching radiofrequency plasma waves Twenty percent thrust efficiency," Sci. 11, 2768 (2021).
34. [34] a. Smolyakov, O. Chapurin, W. Frias, O. Koshkarov, E. Rodanov, T.Tang, M. Umansky, Y. Raitses, I. D. Kaganovich, and V. P. Lakhin, "Fluid theory" Simulation of instability, turbulent transport, and coherent structures In partially magnetized plasma for E×B discharges, "Phys. Controlled Plasma Fusion 59, 014041 (2017).
35. [35] O. Koshkarov, A. Smolyakov, Y. Raitses, and I. Kaganovich, "Self-regulation, Structures, anomalous transport in disordered partially magnetized plasma With intersecting electric and magnetic fields," Phys. Rev. Litt. 122, 18501 (2019).
36. [36] a. T. Boys, J. A. Carlson, ED Kaganovich, E. Right, and A. Smolyakov, "Scaling the frequency of speech rotation within a Benning dump," Phys. plasma 25, 072110 (2018).
37. [37] R. Lucken, A. Tavant, A. Bourdon, M.A. Lieberman, and P. Chabert "Saturation" of magnetic confinement in weakly ionized plasma," Sci. Technol. 29, 065014 (2020).
38. [38] J. Y. Kim, J. Y. Jang, J. Choi, J. Wang, W. I. Jeong, M. A. I. Elgarhy,Goo Jo, K.; Chung and YS Hwang, "Magnetic confinement and instability In partially magnetized plasma, "Plasma Sources Sci. Technol. 30, 025011 (2021).
39. [39] F.W. Sears," Electricity and Magnetism", Addison- Wesley publishing Company ,Inc. , California, 1951.
40. [40] J. R. Reitz ,F. J. Milford, and R. W. Christy, " Foundations of Electromagnetic Theory" , Addison-Wesley publishing Company ,Inc., California, 1979.
41. [41] F.F. Chen and P.C.Jane ,"Lecture Notes on Principle of processing", Plenum Press, (2002)
42. [42] N. Idris, T.N. Usmawanda, K. Lahna, M. Ramli ,"Temperature estimation using Boltzmann plot method of many calcium emission lines in laser plasma produced on river clamshell sample", *IOP Journal of Physics: Conference Series,* 1120, 1, 2018.
43. [43] N. Ohno, M.A. Razzak , H. Ukai , S. Takamura , Y. Uesugi , "Validity of electron temperature measurement by using boltzmann plot method in radio frequency inductive discharge in the atmospheric pressure range", *Plasma Fusion Res*. 1 (2006) 028, 2006.

44. [44] A.M. El Sherbini, A.A.S. Al Aamer, A.T. Hassan, T.M. El Sherbini, "Measurements of plasma electron temperature utilizing magnesium lines appeared in laser produced aluminum plasma in air", *Optics and Photonics Journal*, 2 (2012) 278, 2012.
45. [45] K.H. Spatschek ,"Introduction to Theoretical Plasma Physics," lecture series, 2008.
46. [46] https://www.nist.gov/pml/atomic-spectra-database .
47. [47] N. Konjevic, A. Lesage, J. Fuhr, and W. Wiese,"Experimental Stark widths and shifts for spectral lines of neutral and ionized atoms" , *J. Phys. Chem. Ref. Data*, Vol. 19, No. 6, PP. 1307–1385, 1990.